A dataset of energy, water vapor and carbon exchange observations in oasis-desert areas from 2012 to 2021 in a typical endorheic basin

Shaomin Liu[1], Ziwei Xu[1], Tao Che[2], Xin Li[3], Tongren Xu[1], Zhiguo Ren[2], Yang Zhang[2], Junlei Tan[2], Lisheng Song[4], Ji Zhou[5], Zhongli Zhu[1], Xiaofan Yang[1], Rui Liu[6], Yanfei Ma[7]

Correspondence to: Shaomin Liu (smliu@bnu.edu.cn), Ziwei Xu (xuzw@bnu.edu.cn)

[1]State Key Laboratory of Earth Surface Processes and Resource Ecology, Faculty of Geographical Science, Beijing Normal University, Beijing 100875, China

[2]Northwest Institute of Eco-Environment and Resources, Chinese Academy of Sciences, Lanzhou 730000, China

[3]National Tibetan Plateau Data Center, State Key Laboratory of Tibetan Plateau Earth System and Resources Environment, Institute of Tibetan Plateau Research, Chinese Academy of Sciences, Beijing 100101, China

[4]Key Laboratory of Earth Surface Processes and Regional Response in the Yangtze-Huaihe River Basin, School of Geography and Tourism, Anhui Normal University, Wuhu 241000, China;

[5]School of Resources and Environment, University of Electronic Science and Technology of China, Chengdu 611731, China

[6] Institute of Urban Study, School of Environmental and Geographical Sciences (SEGS), Shanghai Normal University, Shanghai 200234, China

[7]Hebei Technology Innovation Centre for Remote Sensing Identification of Environmental Change, Hebei Key Laboratory of Environmental Change and Ecological Construction, School of Geographical Sciences, Hebei Normal University, Shijiazhuang 050024, China

Abstract:

Oases and deserts generally act as a landscape matrix and mosaic in arid/semiarid regions. The significant difference of thermal and dynamic characteristics between oasis and desert surface will result in oasis-desert interaction. That is, the interaction between oasis and desert system through the exchange of momentum, energy, water and carbon, which can lead to a series of microclimate effects that affect the structure of the atmospheric boundary layer, changes of carbon sources/sinks in oasis and the local ecological environment. Therefore, studying water, heat and carbon exchange is significant for achieving the goals of carbon peaking and carbon neutrality in oasis-desert areas and supporting the ecological security and sustainable development of oases. To monitor energy, water vapor and carbon exchange between the land surface and atmosphere, a land surface process integrated observatory was established in the oasis-desert area in the middle and lower reaches of the Heihe River Basin, the 2nd largest endorheic basin in China. In this study, we present a suite of observational datasets in artificial and natural oases-desert systems, which consist of long-term energy, water vapor, carbon/methane fluxes, and auxiliary data involving hydrometeorology, vegetation and soil parameters from 2012 to 2021. Half-hourly turbulent flux data were acquired by an eddy covariance system and scintillometer. The hydrometeorological data, including radiation, soil heat flux and soil temperature profile, gradient of air temperature/humidity and wind speed/direction, air pressure, precipitation and soil moisture profiles, were observed from automatic weather stations with a 10-minute average period as well as the groundwater table data. Moreover, vegetation and soil

parameters were also supplemented in the datasets. Careful data processing and quality control are implemented during data production, including data collection, processing, archiving and sharing. The current datasets can be used to explore the water-heat-carbon process and its influence mechanism, calibrate and validate related remote sensing products, simulate energy, water vapor and carbon exchange in oasis and desert areas, and provide references and representatives for other similar artificial and natural oases along the Silk Road. The datasets are available from the National Tibetan Plateau Third Pole Environment.

1. Introduction

Arid and semiarid regions represent approximately 30% of the global terrestrial surface area (Dregne, 1991; Scanlon et al., 2006), and dryland expansion occurs under climate change, especially in developing countries (Huang et al., 2015). This proportion is much higher in China, as (semi)arid regions account for approximately 47% of its terrestrial surface (Zhang et al., 2016a; Mao et al., 2018). An oasis is a unique ecological landscape in arid and semiarid areas, which is not only the core of its ecological environment but also the foundation of its economic development, especially in western China, which has been an important part of the ‘Silk Road’ since ancient times. Oases with less than 10% of the total area of arid regions support more than 90% of the population in the arid regions of China (Chu et al., 2005; Li et al., 2016; Zhou et al., 2022). The main geomorphologic feature is a wide sandy desert or Gobi (gravel desert), interspersed with many oases of different sizes and shapes in the middle and lower reaches of a typical endorheic basin in Northwest China (Cheng et al., 1999). The water from upstream is the link connecting these ecosystems, and the oasis is the place where human beings live. The oasis areas are now 3.3 times larger than those in the early 1950s in the region of northwestern China (Zhang et al., 2018). The oasis-desert system plays a crucial role in maintaining a stable ecological environment and agricultural productivity (Zhang and Zhao, 2015). However, inland river basins in arid and semiarid areas are facing the crisis of ecological environment degradation, such as the drying up of rivers and lakes, the degradation of natural vegetation, the intensification of land desertification and the frequent occurrence of dust storms, especially in many inland river basins westward along the Silk Road, such as the Tarim River Basin (Zhao et al., 2013), Aral Sea Basin (Stanev et al., 2004; Crétaux et al., 2009), and Lake Urmia Basin (Stone, 2015). Therefore, it is critical to maintain the balance between the oasis and desert systems to achieve the goal of sustainable oasis development.

The particularity of the underlying surface in the oasis-desert area, e.g., the irrigation cropland, riparian forest, sandy vegetation, seasonal snow and frozen soil, makes the study of land–atmosphere interactions complex and needs comprehensive consideration in such heterogeneous underlying surfaces. The dynamic and thermal characteristics of the underlying surface of the oasis and the desert are significantly different, and the oasis and desert systems interact and influence each other through momentum, energy, water vapor and carbon exchange. Thus, the oasis-desert interaction will affect the structure of the atmospheric boundary layer and the local ecological environment. Additionally, under the influence of weather conditions, the oasis-desert interaction results in the local circulation between oasis and desert and airflows form dynamic and thermal inner boundary layer within the oasis (Cheng et al., 2014). These can lead to the local microclimate characteristics of the oasis-desert area (Liu et al., 2020), such as the wind shield effect and cold-wet island effect of the oasis, the humidity inversion effect within the surrounding desert, and oasis carbon sources/sinks. These microclimate effects play an important role in the self-sustaining and development of oasis systems. Understanding the basic characteristics of energy, water vapor and carbon exchange in oasis-desert ecosystems is important for achieving the goals of carbon peaking and carbon neutrality in the oasis-desert area and supporting ecological security and sustainable development of the oasis.

Extensive studies have investigated energy, water vapor and carbon exchange in oasis-desert areas based on field and remote sensing observations (Taha et al., 1991; Potchter et al., 2008; Xue et al., 2019; Wang et al., 2019; Zhou et al., 2022) and numerical simulations (Chu et al., 2005; Meng et al., 2009; Georgescu et al., 2011; Liu et al., 2020). Li et al. (2016) provided a complete sketch map of oasis and desert interactions based on previous studies, including the oasis cold and wet island effect, oasis wind shield effect (oasis effect), and air humidity inversion effect within the surrounding desert (desert effect), which are important for the stability and sustainability of the oasis-desert ecosystem (Liu et al., 2020). In addition, the oasis-desert areas located in semiarid regions were found to be carbon sinks by previous researchers (Tagesson et al., 2016; Wang et al., 2019), which can significantly affect the carbon balance of arid regions and play an increasingly important role within the global carbon cycle.

The Heihe River Basin (HRB), the second largest endorheic basin in China, is characterized by artificial oases and natural oases in the middle and lower reaches, respectively. Several experiments have been conducted in these oasis-desert areas, e.g., the Heihe River Basin Field Experiment (HEIFE) from 1990 to 1992 to conduct comprehensive studies of atmosphere–land surface interactions over the Zhangye oasis and desert area in the middle reaches of the HRB (Wang et al., 1992), the Jinta experiment from 2005 and 2008 to focus on the energy and water exchange and the atmospheric boundary over the Jinta oasis and desert area in the middle reaches of the HRB (Wen et al., 2012), the oasis-desert area in the middle reaches and mountainous area in upper reaches of watershed allied telemetry experimental research (WATER) and the subsequent HiWATER (oasis-desert area in the middle and lower reaches and mountainous area in upper reaches) to be a comprehensive simultaneous satellite–airborne–ground observations eco-hydrological experiment (Li et al., 2009, 2013). Thereafter, a multielement, multiscale, networked, and elaborate integrated observatory network was established in the oasis-desert area in the middle and lower reaches and mountainous area in upper reaches of the HRB since 2007 and completed in 2013 (Liu et al., 2018). A quantitative understanding of the energy, water vapor and carbon exchange in oasis-desert areas is crucial for recognizing the oasis-desert interactions and is significant for protecting the ecological stability and socioeconomic development of oases, and long-term observations are indispensable. The observations and research findings from the oasis-desert area in the HRB will serve as references and representatives for other similar artificial and natural oases along the Silk Road. To achieve the aforementioned objective, observations should be continuously conducted, and a high-quality dataset should be obtained.

In this paper, the integrated observatory network of the artificial and natural oasis-desert areas in the middle and lower reaches in the HRB are introduced first, and the observations characterizing the energy, water vapor and carbon exchange are detailed explicated, which provides a 10-year dataset. Specifically, the spatial distribution and design of the observation sites are summarized in Section 2. Section 3 describes the data processing and quality control procedures. In Section 4, the energy, water vapor and carbon fluxes and related auxiliary parameters are introduced in detail. The data availability is documented in Section 5, and the conclusions are summarized in Section 6. This dataset can be used for comprehensive understanding of energy, water vapor and carbon exchange in oasis-desert areas, and validating simulation results and remote sensing products of energy, water vapor and carbon fluxes in oasis-desert areas.

2. A land surface process integrated observatory network in the oasis-desert area of the HRB

2.1 Study area description

The study areas are the middle and lower reaches of the HRB, which are located in the arid regions of western China, provided by water from the typical cryosphere of the upper reaches. In the upper reaches, glaciers, snow cover and frozen ground is widely distributed and snowfall could occur in any season (elevation >3800 m). The typical snow depth is 15-30 cm with a duration of 90-120 days in the snow-covered regions (Che et al., 2012; Che et al., 2019). The middle reaches, typical of the artificial oasis-desert system in Zhangye City, the largest oasis in the Hexi Corridor, cover an area of 29,717 km^2 with an oasis area of 5,560 km^2, while the lower reaches in Ejina Banner have a natural oasis-desert system covering an area of 85,678 km^2 with an oasis area of 1,130 km^2 (Fig. 1). Among the oases, agricultural oases can be traced to the history of more than 2000 years. The annual average air temperature was 7.29 °C and 9.75 °C, and the annual accumulated precipitation was 184.83 mm and 37.31 mm (1979-2018) in the middle and lower reaches, respectively.

Eleven land surface fluxes and meteorological stations have been established in these regions since 2012 with two superstations and eleven ordinary stations (Table 1; Section 2.2), specifically two oasis stations and three desert stations in the middle reaches and five oasis stations and one desert station in the lower reaches.

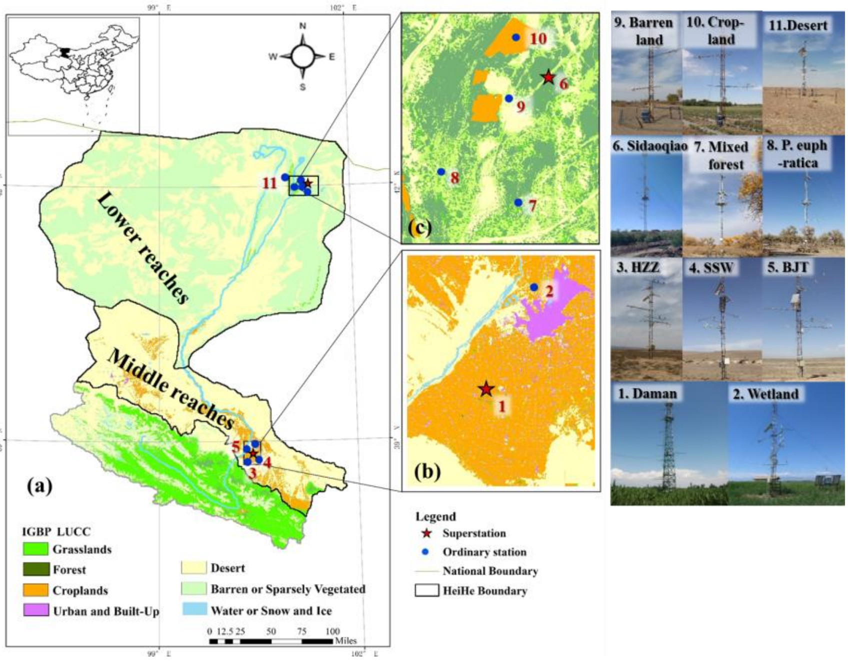

Fig. 1. The middle and lower reach observation systems in the HRB. (a: Heihe River basin; b: Stations in the Zhangye artificial oasis-desert area in the middle reaches; c: Stations in the Ejina natural oasis area in the lower reaches)

Table 1. Station information in the middle and lower reaches of the HRB

ID	Name	Longitude (°, E)	Latitude (°, N)	Elevation (m)	Land Cover	Duration	Location
1	Daman	100.37	38.86	1556	Maize	May 2012-present	Oasis in midstream, superstation
2	Zhangye Wetland	100.45	38.98	1460	Wetland mainly reed	June 2012-present	Oasis in midstream, ordinary station
3	Huazhaizi Desert Steppe	100.32	38.77	1731	*Kalidium foliatum*	June 2012-present	Desert in midstream, ordinary station
4	Shenshawo Sandy Desert	100.49	38.79	1594	Sandy	June 2012-Apr.2015	Desert in midstream, ordinary station
5	Bajitan Gobi	100.30	38.92	1562	Reaumuria	May 2012-Apr.2015	Desert in midstream, ordinary station
6	Sidaoqiao	101.14	42.00	873	*Tamarix*	July 2013-	Oasis in downstream,

						present	superstation
7	Mixed Forest	101.13	41.99	874	*Populus euphratica and Tamarix*	July 2013-present	Oasis in downstream, ordinary station
8	Populus euphratica	101.12	41.99	876	*Populus euphratica*	July 2013-Apr.2016	Oasis in downstream, ordinary station
9	Barren Land	101.13	42.00	875	Bare land	July 2013-Mar.2016	Oasis in downstream, ordinary station
10	Cropland	101.13	42.00	875	Melon	July 2013-Nov.2015	Oasis in downstream, ordinary station
11	Desert	100.99	42.11	1054	Reaumuria	Apr.2015-present	Desert in downstream, ordinary station

2.2 Observation systems

2.2.1 Artificial oasis and desert areas in the middle reaches

The middle reaches are located in the Zhangye oasis in Zhangye City of Gansu Province, and the primary underlying surfaces include cropland (maize), shelterbelt, orchard, residential area and wetland (reed) in the oasis and sandy desert, desert steppe (*Kalidium foliatum*), and the Gobi Desert (Reaumuria) in the surrounding desert. Five stations (one superstation and four ordinary stations) were established in these surfaces, which are representative of the main underlying surface types within the oasis-desert area in the middle reaches of the HRB.

There is one superstation (maize and shelterbelt) and one ordinary station (wetland and reed) in the Zhangye oasis surrounding three ordinary stations in the desert located in the middle reaches of the HRB (Fig. 2a). The superstation includes a multiscale observation system for energy, water vapor and carbon fluxes (lysimeter-EC system-scintillometer for meter-hundred-kilometer observation scale) and soil moisture measurements (*in situ* soil moisture profile-cosmic ray probe-soil moisture wireless sensor network for meter-hundred-kilometer observation scale), and it includes a hydrometeorological gradient observation system to monitor the profile (7 layers) of wind speed/direction, air temperature/humidity and carbon dioxide and water vapor concentration, one layer four-component radiation, air pressure, precipitation, and infrared temperature (2 repetitions), 9/8 layers' soil temperature/moisture profile, soil heat flux (3 plates with two buried under the bare soil between two corn plants and one buried under the corn plants), etc. The EC and hydrometeorological gradient observation system were installed on a 40 m tower. Optical and microwave scintillometers were installed on both sides of the 40 m tower apart from 1854 m. There were also observations of vegetation parameters in the 40 m tower, including a visible and near infrared phenological camera to monitor the vegetation index and crop growth curve, two photosynthetically active radiation (PAR) sensors to monitor PAR, a vegetation chlorophyll fluorescence observation system to monitor sun-induced chlorophyll fluorescence (SIF), and an LAI wireless sensor network (28 nodes) to monitor multipoint LAI in the source area of the scintillometer (Fig. 2b, Fig. 4a).

The ordinary stations are comprised of an EC system, an automatic weather station (AWS) and a visible and near infrared phenological camera. The observation elements of the AWS include two layers' air temperature/humidity and wind speed/direction, one layer's four-component radiation, air pressure, and infrared temperature (2 repetitions), two layers' precipitation, 8/7 layers' soil temperature/moisture, soil heat flux (3 plates), etc. (Fig. 2c).

The sonic anemometers of the ECs were installed at a height of approximately 3-7 m above the canopy to capture the sensible heat, latent heat, carbon dioxide and methane (in wetland) fluxes, etc. The sonic anemometers of all the ECs were aimed toward the north. Soil parameters, such as soil texture, porosity, bulk density, saturated hydraulic conductivity, and soil organic matter content, etc. were investigated at each station in 2012 and 2020. Detailed information can be found in Table 2.

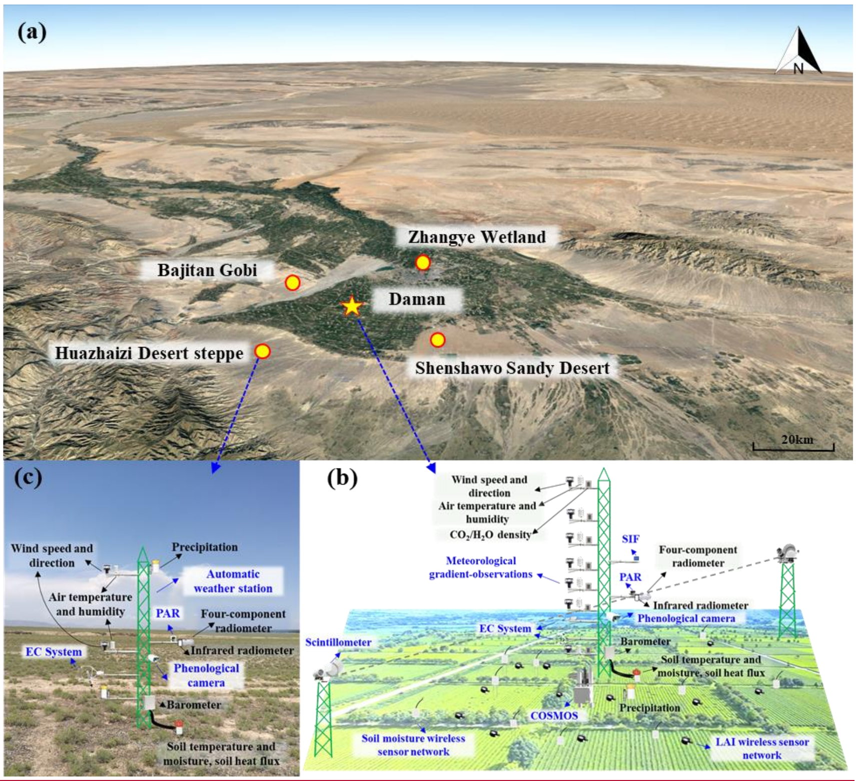

Fig. 2. Sketch map of the artificial oasis and desert area in the middle reaches (a: artificial oasis and desert area (from © Google Earth); b: Daman superstation; c: Huazhaizi ordinary station)

2.2.2 Natural oasis and desert areas in the lower reaches

The Ejin Banner oasis is located in the lower reaches of the HRB and belongs to Inner Mongolia and part of Jiuquan city of Gansu Province, which is surrounded by widespread desert. The main underlying surfaces were Reaumuria and terminal lake in desert, riparian forest, cropland, barren land and residential area in the oasis in the lower reaches. There were six stations (one superstation and five ordinary stations) in the lower reaches, which are located in these land covers, including *Populus euphratica*, *Tamarix chinensis*, cropland, barren land, and desert.

In the oasis-desert area of the lower reaches, there is one superstation and four ordinary stations in the oasis and one ordinary station in the desert (Fig. 3a). The superstations include a multiscale observation system for energy, water vapor and carbon fluxes (sap flow gauge-EC-large aperture scintillometer for meter-hundred-kilometer observation scale) and soil moisture measurements (*in situ* soil moisture profile and cosmic ray probe for meter and hundred meter observation scale), a hydrometeorological gradient observation system to monitor the profile (6 layers) of wind speed/direction, air temperature/humidity, one layer four-component radiation, air pressure, and infrared temperature (2 repetitions), two layers of precipitation, 10/9 layers soil temperature/moisture profile, soil heat flux (with two buried under the bare soil and one buried under the *Tamarix* plants), etc. The EC and hydrometeorological gradient observation system were installed on a 28 m tower. Two groups of large aperture scintillometers were installed on both sides of the 28 m tower apart from 2350 m. The vegetation parameter observations included PAR and the phenological camera to monitor the vegetation index and crop growth curve installed in the 28 m tower and LAI wireless sensor network (11 nodes in the source area of the scintillometer) (Fig. 3b, Fig. 4b). The ordinary stations are comprised of an EC system, an AWS and a visible and near infrared phenological camera. (Fig. 3c).

Additionally, thermal infrared radiometers and imagers were installed at the Mixed Forest and Sidaoqiao stations to measure different component temperatures, i.e., the brightness temperature of different land cover types under different illumination conditions (Li et al., 2019). The soil parameters and groundwater table were observed around the stations. Detailed information can be found in Table 2.

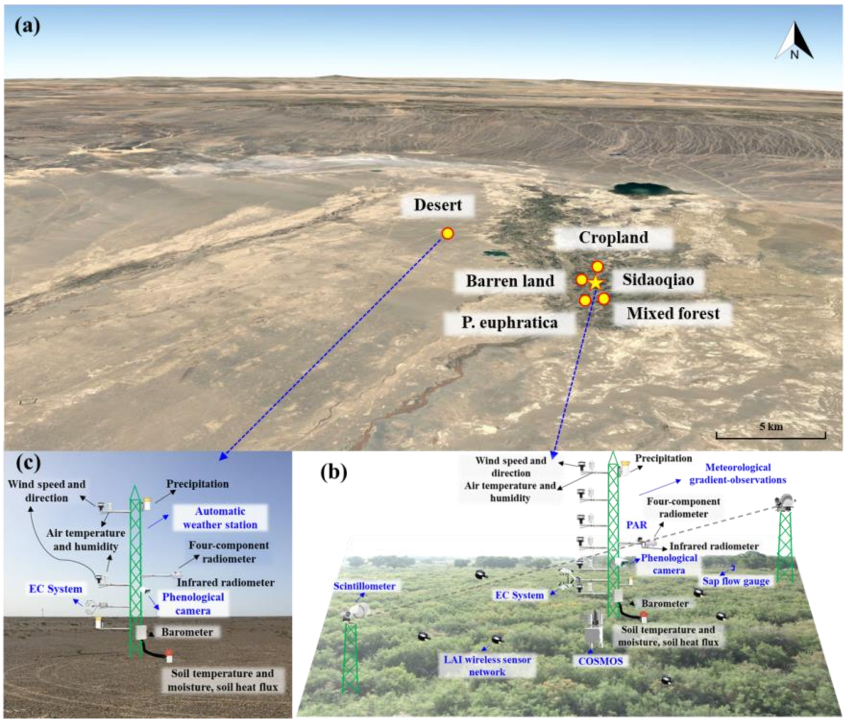

Fig. 3 Sketch map of the natural oasis and desert areas in the lower reaches (a: natural oasis and desert area (from © Google Earth); b: Sidaoqiao superstation; c: desert

ordinary station)

Table 2 Observation variables and sensor configurations of surface flux, hydrometeorology, vegetation and soil parameters

Observations	Sensor	Manufactory	Height/depth (m)	Sites
Surface flux observations:				
Sensible heat, latent heat, carbon dioxide, methane flux	CSAT3&Gill, Li7500&Li7500 A&Li7500DS& EC155&Li7700 CPEC310	Campbell and LiCor, USA	3~7 m above the canopy	All stations (methane observation only in wetland, closed path EC at Daman and Desert, stations)
Sensible and latent heat flux	BLS900 and MWSC-160	Scintec and RPG, Germany	23.92	Daman
	BLS900	Scintec, Germany	25.5	Sidaoqiao
Sap flow	TDP 30	Rainroot, China	1.5	Mixed forest
Hydrometeorological observations:				
Pressure	PTB110	Vaisala, Finland	--	Bajitan, Shenshawo
	AV-410BP	Avalon, USA	--	Mixed Forest
	PTB210	Vaisala, Finland	--	Huazhaizi
	CS100	Campbell, USA	--	Daman, Wetland, Sidaoqiao, Desert
Precipitation	TE525MM	Texas Electronics, USA	--	Daman, Wetland, Huazhaizi, Bajitan, Shenshawo,Sidaoqiao, Desert
	52203	RM Young, USA	--	Mixed Forest
Wind speed/direction	Windsonic	Gill, UK	3,5,10,15,20,30,40	Daman,
			5,7,10,15,20,28	Sidaoqiao
			5,10	Wetland, Huazhaizi, Mixed forest
	010C/020C	Met One	5,10	Wetland, Desert
	03001	RM Young, USA	10	Bajitan,Shenshawo
			28	Populus euphratica
Air temperature/hu	HMP45D	Vaisala, Finland	28	Mixed Forest

midity	HC2S3	Vaisala, Finland	5,7,10,15,20,28	Sidaoqiao
	HMP45AC	Vaisala, Finland	5,10	Bajitan,Huazhaizi, Shenshawo,Wetland, Desert
			28	Populus euphratica
	AV-14TH	Avalon	3,5,10,15,20,30,40	Daman
Four-component radiation	CNR4	Kipp&Zonen, Netherland	10 22	Sidaoqiao Mixed Forest
	CNR1	Kipp&Zonen, Netherland	6	Wetland,Huazhaizi,Bajitan,Shenshawo,Desert,Barren land, Cropland
			22	Populus euphratica
	PSP&PIR	Eppley, USA	12	Daman
Infrared temperature	SI-111	Apogee, USA	12	Daman
			10	Sidaoqiao
			22	Populus euphratica, Mixed Forest
			6	Wetland,Huazhaizi,Bajitan,Shenshawo,Desert,Barren land, Cropland
Soil temperature profile	109ss-L	Campbell, USA	0,-0.02,-0.04,-0.1,-0.2,-0.4,-0.8,-1.2,-1.6,-2.0	Sidaoqiao,
			0, -0.02,-0.04,-0.1,-0.2,-0.4,-0.6,-1.0	Desert Wetland
	AV-10T	Avalon, USA	0, -0.02,-0.04,-0.1,-0.2,-0.4,-0.6,-0.8,-1.2,-1.6	Daman
			0, -0.02,-0.04,-0.1,-0.2,-0.4,-0.6,-1.0	Bajitan, Huazhaizi
			0, -0.02,-0.04,-0.1,-0.2,-0.4	Wetland
			0,-0.02,-0.04,-0.1,-0.2,-0.4,-0.6,-1.0,-1.6,-2.0,-2.4	Mixed forest
	109	Campbell, USA	0, -0.02,-0.04,-0.1,-0.2,-0.4,-0.6,-1.0	Shenshawo
			0, -0.02,-0.04	Barren land, Cropland, Populus euphratica

Soil moisture profile	ECH_2O-5	Decagon Devices, USA	-0.02,-0.04,-0.1,-0.2,-0.4,-0.6,-1.0	Bajitan
	CS616	Campbell, USA		Shenshawo, Desert
			-0.02,-0.04,-0.1,-0.2,-0.4,-0.6,-0.8,-1.2, -1.6	Daman
	ML2X	Delta-T, UK	-0.02,-0.04,-0.1,-0.2,-0.4,-0.8,-1.2,-1.6,-2.0	Sidaoqiao
			-0.02,-0.04,-0.1,-0.2,-0.4,-0.6,-1.0,-1.6,-2.0,-2.4	Mixed Forest
			-0.02, -0.04	Barren land, Populus euphratica, Cropland
	ML3	Delta-T, UK	-0.02,-0.04,-0.1,-0.2,-0.4,-0.6,-1.0	Desert, Huazhaizi
Soil heat flux	HFP01	Hukseflux, Netherland	-0.06	Wetland,Huazhaizi, Bajitan,Shenshawo,Desert,Barren land, Cropland
	HFT3	Campbell, USA		Bajitan, Populus euphratica, Mixed forest
	HFP01SC	Hukseflux, Netherland		Daman, Sidaoqiao
Averaged temperature	TCAV	Campbell, USA	-0.02, -0.04	Daman, Sidaoqiao
CO_2/H_2O profile	AP200	Campbell, USA	3,5,10,15,20,30,40	Daman
Groundwater Table	U20	Onset, USA	-2~-3m	Sidaoqiao, Mixed forest, Populus euphratica, Cropland, Desert
Vegetation parameter observations:				
Vegetation phenology	Phenological camera	XST-PhotoNet, China	above the canopy	All sites
LAI	XST- LAINet	Beijing StarViewer Science and Technology Ltd., China	Below the canopy	28 nodes around Daman, 6 nodes around Sidaoqiao, 5 nodes around Mixed forest
photosynthetically active radiation	PQS-1	Kipp&Zonen, Netherland	0.5, 12	Daman
			10	Sidaoqiao
			22	Mixed forest, Populus euphratica
			6	Wetland, Cropland

Sun-induced chlorophyll fluorescence	AutoSIF-1	Beijing Bergsun Spectral Technology Co. Ltd, China	34	Daman
Soil parameters: soil sampling and laboratory testing in 2012 and 2020				

3. Data processing and quality control

The data processing and quality control procedure can be divided into data collection, data processing and data archiving and sharing (Fig. 4).

In the data collection step, the comparison and calibration of instruments are prerequisites to ensure the quality of the observation data. The instrument comparison experiments were specifically arranged under the Gobi Desert in 2012 in the middle reaches (Xu et al., 2013) and shrub in 2013 in the lower reaches (Li et al., 2018) to ensure the consistency and comparability of the instruments. In addition, the instruments with multiple layers were compared at the same height before installation, the soil moisture probes were also compared under dry and wet conditions, and the multitype rain gauges were compared in the same field. The infrared gas analyzer of all the EC systems was calibrated at the beginning and end of the vegetation-growing season every year. To ensure the data quality, a routine maintenance procedure is formulated and strictly followed, including daily (checking the real-time data through remote monitoring and data management system for field observatory network v1.0), 10 days (checking the time series plot providing by the system), monthly (routine inspection in every station), and annually (data processing and release) (Liu et al., 2018). The Heihe watershed internet of things observation system was developed to complete the above maintenance procedure, which included remote receiving and storing the filed data, browsing and processing real-time data, monitoring the instrument status and early warning the abnormal conditions, etc.

During the data processing step, a processing scheme was formulated for each type of instrument. For the EC system, the data were processed from the raw 10 Hz turbulent data, including spike detection, sonic temperature correction, coordinate rotation, frequency response correction, and WPL (Webb-Pearman-Leuning) correction. (Liu et al., 2016; Wu et al., 2023). Additionally, the 30-min flux data series were identified as quality flags according to the stationarity test and integral turbulence characteristics test. A final quality flag (1~9) was assigned to each specific turbulent flux value, indicating good quality (1~3), suitability for general use (4~6), poor but better than gap filling data (7~8), and discarded data (9). The unclosed energy balance of EC system is a universal problem. There was approximately an average of 17% energy imbalance in our study area (Xu et al., 2017; Zhou et al., 2018), which was reasonable compared with previous results (Stoy et al., 2013). The Bowen-ratio correction method is recommended to close the energy balance (Twine et al., 2000; Xu et al., 2020). The data processing steps from scintillometer measurements to surface fluxes are as follows: raw data to light intensity variance, light intensity variance to the structure parameter of the refractive index of air (C_n^2), C_n^2 to meteorological data, and finally obtaining surface fluxes combining the meteorological data. Four steps are taken to ensure the quality of scintillometer data (Liu et al. 2011; Zheng et al., 2023): (i) excluding data for C_n^2 beyond the saturation criterion; (ii) excluding data obtained during periods of precipitation; (iii) excluding data when the demodulated signal is small; and (iv) excluding data when the sensor is malfunctioning. The steps of the meteorological gradient observation system and AWS data processing and quality control were twofold: (1) all the AWS data were averaged over an interval of 10 min for a total of 144 records per day. The missing data were denoted by -6999; (2) the unphysical data were rejected, and the gaps were denoted by -6999. The surface soil heat flux was calculated using the 'PlateCal' approach (Liebethal et al., 2005), and the final surface soil heat flux was the weighted vegetation fraction combined with the soil temperature and moisture measured above the heat plates. There are approximately 10–20% missing or rejected values of EC or scintillometer data. The look-up table (LUT) method is recommended to fill the gaps when data were missing (Xu et al., 2020). The maximum missing values of AWS data were no more than 10%, and linear interpolation method is recommended to fill the missing values. The vegetation growth curve and vegetation index can be obtained from visible and near infrared bands measured by phenological cameras. The key phenological parameters are determined according to growth curve fitting, such as the growth season start date, peak, and growth season end. The leaf area index (LAI) data were obtained from the LAINet sensor, which can continuously measure the multipoint total solar radiation above the canopy and the transmitted radiation below the canopy, and the LAI was calculated based on multiangle transmittance data (Qu et al., 2014). Seven days moving averaged method is recommend to eliminate noise from the daily LAI observations (Qu et al., 2014). Then, all the data are processed into a standardized file for sharing.

During the archiving and sharing step, the metadata were written for each data point, including the site description, processing step, header description, and other notes. (Li et al., 2017a). Before data are released, self-examination, crosschecks and expert review are required to ensure data quality. Finally, the data were archived and shared online.

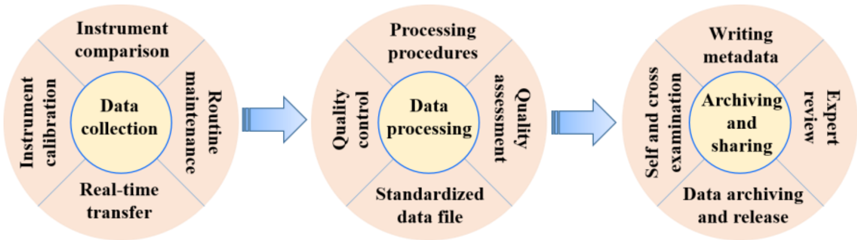

Fig. 4 Flowchart of data processing and quality control

4. Data description

4.1 Energy, water vapor and carbon fluxes data

The EC systems were used to measure surface flux at all sites, namely, 5 stations (2 in oasis, 3 in desert) in the middle reaches and 6 stations (5 in oasis, 1 in desert) in the lower reaches. The turbulent flux data were recorded by the open path or closed path EC systems and processed carefully. In addition to the surface flux of sensible, latent and carbon dioxide, the methane flux was also observed at the wetland site in the middle reaches (Table 2). The multiyear seasonal variations in sensible heat, latent heat, carbon dioxide and methane fluxes are shown in Figure 5. Generally, the latent heat fluxes in oases are obviously higher than those in deserts, especially in the lower reaches. The latent heat fluxes exhibited a single peak during one year, with a peak value of approximately 200 W m^{-2} in the oasis area; however, they significantly fluctuated due to irrigation (normally 4 times in cropland of the midstream region, 2 times in riparian forest and melon of the downstream region) or precipitation. In the middle reaches, the latent heat flux in the wetland showed the largest values, which were more than 200 W

m^{-2} in the crop growing season, and it also presented relatively large values in the midstream piedmont desert region with dense *Kalidium foliatum* cover (peak value greater than 50 W m^{-2}). In the lower reaches, the latent heat flux showed consistent variations in the riparian forest with a peak value of approximately 150 W m^{-2} during the crop growing season; however, it showed large fluctuations in the melon surface during growth due to frequent irrigation (approximately 7~8 times), and the bare land in the oasis and desert had a small latent heat flux.

The seasonal variations in sensible heat flux were totally different in the oasis and desert systems. The sensible heat flux showed two peaks in the oasis in both the middle and lower reaches except for the bare land, namely, reaching maximum values at the end of April and September, and it showed minimum values in mid-August (-25 W m^{-2}), corresponding to large values of latent heat flux in the oasis that were even greater than net radiation. This phenomenon was also found by previous researchers (Liu et al., 2011) and was called the 'oasis effect'. In the desert area, the sensible heat flux appeared as a single peak in spring and decreased gradually since then. The variation in sensible heat flux in bare land of the natural oasis in the lower reaches is similar to that in the desert area.

In the oasis, the carbon dioxide (CO_2) flux showed obvious 'U' variations, especially in the middle reaches. The crop absorbed carbon dioxide (carbon sink) in the crop-growing season, and a negative value of approximately -14 μmol m^{-2} s^{-1} was observed in the maize surfaces. The magnitude of the methane (CH_4) flux was lower than the CO_2 flux and was in the range of approximately 0~0.1 μmol m^{-2} s^{-1} in the wetland. The CH_4 flux in the non-growing season was the lowest and increased rapidly in April. Although the magnitude of the CH_4 flux was lower than the CO_2 flux, the contribution of methane emissions to global warming was as important as CO_2 contributions on a long time scale (Hommeltenberg et al., 2014; Zhang et al., 2016b), especially focusing on CH_4 flux measurements in wetlands (Zhang et al., 2022). The variations in CO_2 flux in the riparian forest were relatively small, with values of approximately -0.4 μmol m^{-2} s^{-1} in the plant growing season. There was little carbon sequestration in the desert area due to little or sparse vegetation, and the CO_2 flux in the desert area was very small, fluctuating around zero during the years.

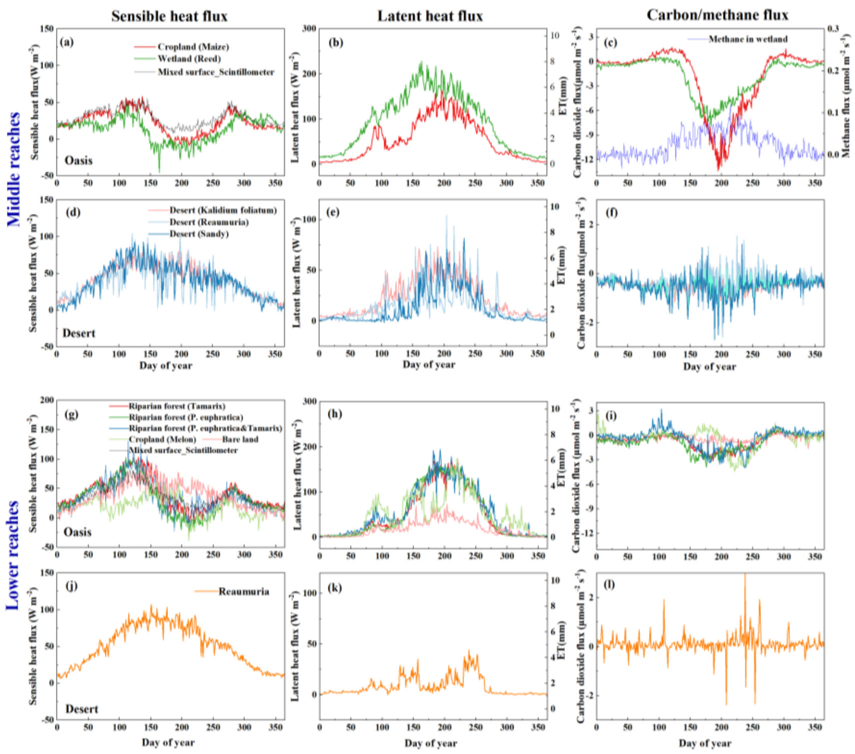

Fig. 5 The multiyear seasonal variations in sensible, latent heat, carbon dioxide and methane fluxes in the oasis-desert area (sensible heat flux—left, latent sensible heat flux—middle, carbon dioxide and methane flux—right, 2012-2021)

4.2 Hydrometeorological data

The hydrometeorological data were obtained from 13 AWSs, with six in the middle reaches (Fig. 2) and seven in the lower reaches (Fig. 3) of the HRB. All the AWSs recorded four-component radiations (short/long wave upward and downward radiation), soil heat flux, surface and soil temperature profiles, air temperature and humidity, wind speed and direction, air pressure, precipitation, soil moisture profiles, infrared temperature, and groundwater table in the lower reaches~~, etc~~. (Table 2). All sensors were calibrated and intercompared before being mounted. The sampling frequencies, reference heights and directions of these sensors at all stations were identical to maintain consistency.

4.2.1 Radiation, soil heat flux, surface and soil temperature profile

带格式的：字体：加粗

It is important to understand the variations in radiation and surface soil heat flux in oasis and desert areas, which are the surface available energy. Figure 6 shows the four radiation components and soil heat flux in oasis and desert areas in the middle and lower reaches in the HRB, and all the variables exhibited obvious seasonal variations with an inverted ‘U’ shape. The incoming shortwave radiation was consistent with each other in oasis and desert because of the short distance among the sites. Due to the higher albedo in the desert, the upward shortwave radiation in the desert was larger than that in the oasis (approximately larger than 30%). The incoming longwave radiation originates from the atmosphere (in particular CO_2 and water vapor) and thermal radiation of clouds in the lower atmosphere. The oasis presents relatively large water vapor and cloudiness; thus, the incoming longwave radiation for the oasis was greater than that for the desert (approximately 2%). It is to be expected that under dry conditions during the daytime, the surface temperature of the desert will be significantly greater than that of the well-watered oasis site. Consequently, the upward longwave radiation in the desert was larger than that in the oasis (approximately 8%). The net radiation, driving the turbulent fluxes of sensible heat and latent heat at the earth surface and heating soil, was greater in the artificial oasis and the natural oasis than in the desert at approximately 50 W m^{-2}. The daily mean surface soil heat fluxes varied similarly in oasis and desert areas with relatively low values in the range of -20 to 20 W m^{-2}.

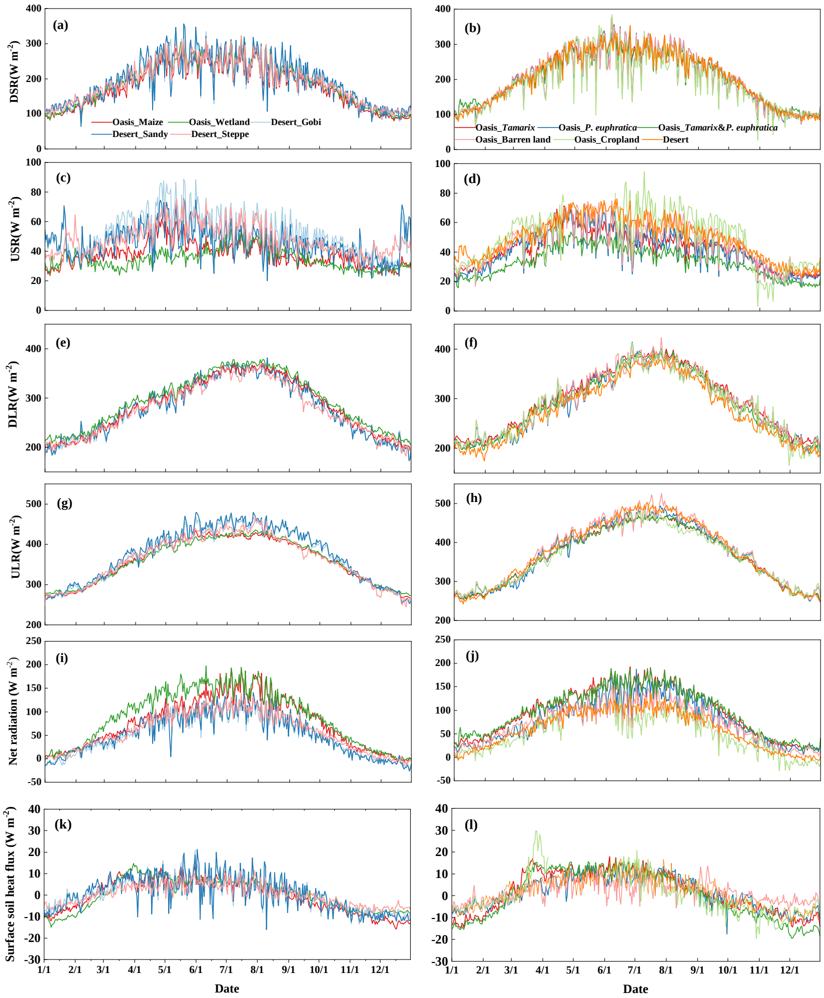

Fig. 6 Seasonal variations in multiyear average radiation components in the oasis-desert system (middle reaches: a, c, e, g, i, k; lower reaches: b, d, f, h, j, l; 2012-2021 daily averaged DSR: downward shortwave radiation; USR: upward shortwave radiation; DLR: downward longwave radiation; ULR: upward longwave radiation)

The soil temperature exhibited a signal peak around the year in the range of -15°C~34°C, and it decreased with increasing soil depth during the plant growing season; however, it exhibited an increasing trend in the winter. The shallow soil began to thaw at the beginning of spring (march) and to freeze in autumn (November). The soil temperature changed little with depth when it exceeded 0.8 m and 1 m in the oasis and desert, respectively. The soil temperature in the desert was significantly higher by approximately 10 °C during the plant growing season than that in the oasis in both the middle and lower reaches. Additionally, the soil temperature in the artificial oasis-desert area (middle reaches) was approximately 5 °C lower during the plant growing season than that in the natural oasis-desert area (lower reaches) (Fig. 7).

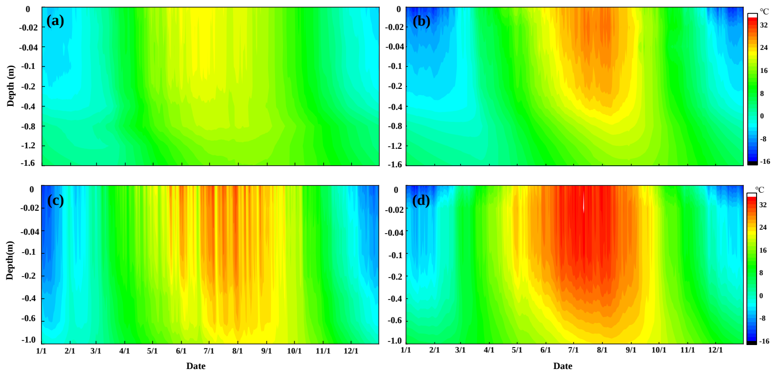

Fig. 7. Seasonal variations in surface and soil temperature profiles in oasis and desert areas (2012-2021) (a: oasis in middle reaches–maize; b: oasis in lower reaches–*Tamarix*; c: desert in middle reaches–Reaumuria; d: desert in lower reaches–Reaumuria)

4.2.2 Air temperature/humidity, wind speed/direction, air pressure

带格式的：字体：加粗

To show micrometeorological characteristics clearly, the comparison of daily average air temperature and relative humidity (5 m except the *P. euphratica* surface with a height of 28 m), wind speed (10 m) and air pressure in desert and oasis are plotted in Figure 8. The seasonal variation in air temperature in the oasis and desert was similar; however, the air temperature in the desert was generally higher than that in the oasis by approximately 0.6 °C on average annually (approximately 0.4 °C in the plant growing season). Instead, the relative humidity in the desert was lower than that in the artificial oasis in the midstream region (approximately 9% and 10% in the annual and plant growing seasons, respectively). The relative humidity in natural oasis and desert areas are similar due to the extreme arid regions with rare precipitation, little irrigation amount and small natural oasis area. Generally, the desert surface has the characteristics of high temperature and lower humidity, and the oasis is a cold and wet island. In the middle and lower reaches of the oasis and desert areas, the wind speed in the desert was obviously larger than that in the oasis because of the wind shield effect in the oasis (middle reaches: 1~3 m/s in the oasis, 2~6 m/s in the desert; lower reaches: 3~6 m/s in the oasis, 3~7 m/s in the desert), and the wind speed decreased significantly when passing by the windbreaks, buildings and crops, especially in the artificial oasis in the middle reaches. The lower wind speed in oases is helpful to plant growth, people's survival environment and the maintenance of oasis and desert ecosystems (Wang and Cheng, 1999). While the seasonal variation in wind speed between desert and oasis was similar, this indicated that they were controlled by the same synoptic system. The wind speed in the natural oasis in the lower reaches was higher than that in the artificial oasis in the middle reaches. The maximum wind speeds were observed in April in the artificial and natural oases, respectively, while the minimum values were observed in July. The air pressure decreased with decreasing elevation, e.g., the air pressure in the middle reaches with relative high elevation was lower than that in the lower reaches, as well as the discrete distribution of stations in the middle reaches with different elevations (Fig. 10g and h, Table 1).

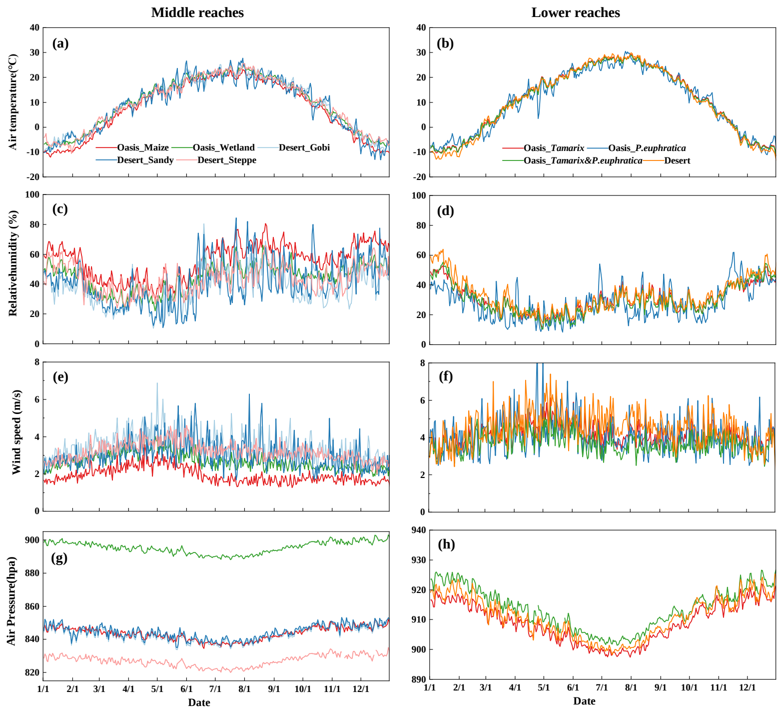

Fig. 8 Micrometeorological comparison between the oasis and desert (a, b: air temperature; c, d: relative humidity; e, f: wind speed; g, h: air pressure, 2012-2021)

Windbreaks, buildings, crops or riparian forests drag on the wind flow inside the oasis, and the wind direction is different in the oasis and desert. In the middle reaches, the dominant wind directions in the desert are the northwest wind and southeast wind directions, while they are northwest and southwest (10 m) in the oasis cropland; however, with the increase in observation height, the influence of surface roughness on wind speed/direction decreased, and the southwest wind gradually decreased, while the northwest wind and southeast wind gradually increased, which is similar to the wind in the desert area around the oasis (~30 m height). In the lower reaches, the wind direction was similar in the oasis and desert areas, with prevailing wind directions of west and east (Fig. 9).

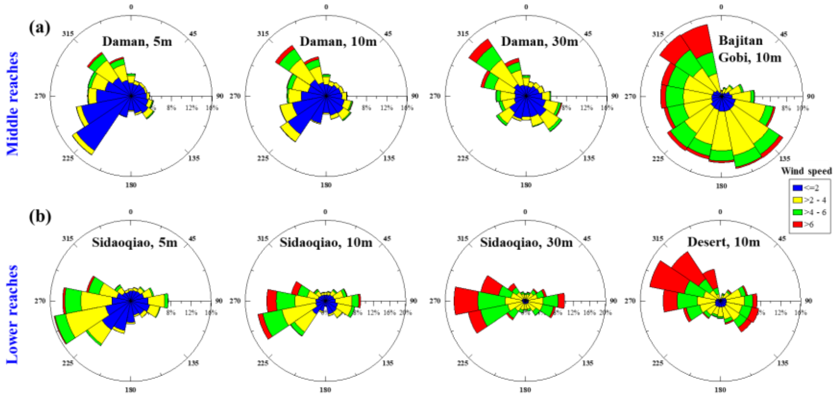

Fig. 9 Wind speed/direction in the oasis and desert area (2012-2021) (a: artificial oasis-desert area in middle reaches; b: natural oasis-desert area in lower reaches; legend is wind speed)

There are six/seven layer gradient observations of wind, air temperature and humidity in superstations in artificial and natural oases. Data on typical days during January, April, July and October in 2021 were selected, and the profiles of wind speed, air temperature and humidity are plotted in Fig. 10. The wind speed generally increased with the observation height, especially in the natural oasis. The air temperature showed inversion at night during atmospheric stable stratification and changed little even below 10 m in the afternoon in July at both artificial and natural oases, which may be caused by oasis-desert interactions. The relative humidity was low during the daytime and maintained high values at night, decreasing with the observation height, especially below 10 m.

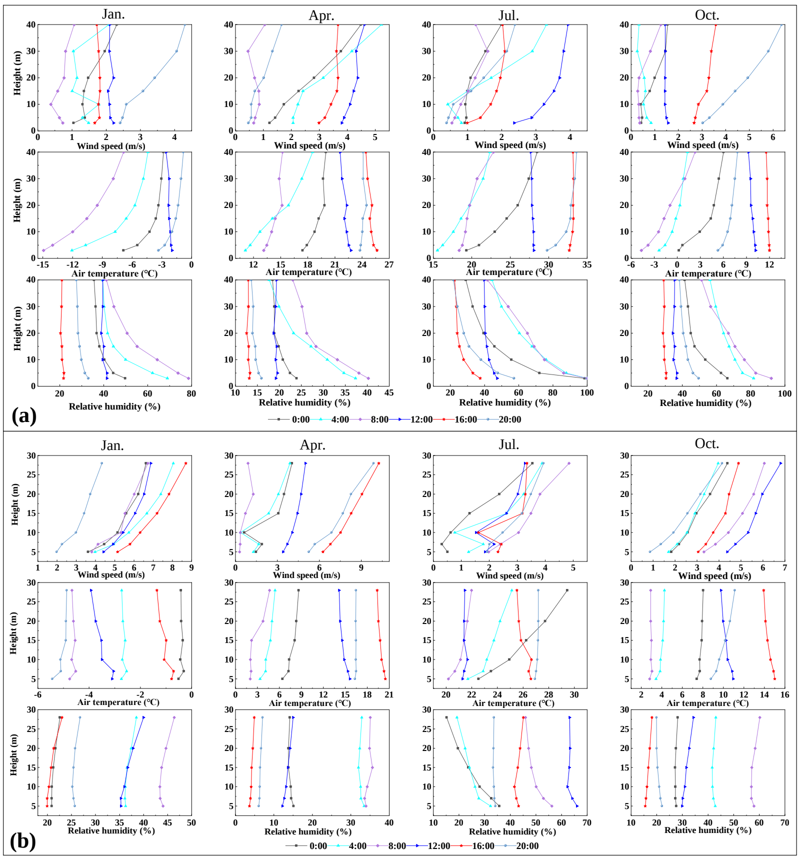

Fig. 10 The profile of wind speed, air temperature and relative humidity in typical days of January 14, April 14, July 14 and October 14 in 2021 (a: artificial oasis in middle reaches; b: natural oasis in lower reaches)

4.2.3 Precipitation, soil moisture and groundwater table

带格式的：字体：加粗

Figure 11 shows the variations in precipitation, soil moisture profiles and groundwater table (lower reaches) in typical oasis and desert ecosystems. Precipitation in the middle reaches was higher than that in the lower reaches, and it was higher in the oasis than in the desert. The soil moisture in the oasis was significantly higher than that in the desert, and it was especially small in the desert of the lower reaches. The soil moisture exhibited an increasing trend with increasing soil depth, especially in the oasis. The soil moisture was higher at depths of 0.8-1 m in the artificial oasis in the middle reaches and at depths of 0.4-0.8 m in the natural oasis in the lower reaches. Soil crust appeared in the lower reaches due to soil salinization, and it may prevent the loss of soil moisture. When a precipitation event occurred, the soil moisture in the desert increased accordingly; however, there were no clear variations in the oasis. There were usually four irrigation events in the artificial oasis in the middle reaches, and the soil moisture increased clearly accordingly, while some occasional peaks in soil moisture were due to relative heavy precipitation (Fig. 11a). In the lower reaches, two irrigation events (usually in March and September) generally occurred in riparian forests in natural oases. The shallow soil moisture showed large values in March when irrigation occurred and decreased in the plant growing season with a slight increase in September. Another phenomenon is that the precipitation in the artificial oasis was larger than that in the desert, although the sites were not far away from each other (e.g., 103.1 mm at the Daman superstation and 75.4 mm at the Gobi station). From the analysis, the soil moisture in the desert was strongly dependent on precipitation (Fig. 11c, d), while it maintained high values in the plant growth season relying on irrigation in the oasis.

In the lower reaches, five systems for groundwater table measurement have operated since June 2014 in the oasis, near the Sidaoqiao, Mixed Forest, *Populus euphratica*, Cropland, and Barren Land stations. The groundwater table was approximately 1–3 m under the ground, and the groundwater table level declined from a depth of approximately 1 m to 3 m in the growing season to supply the riparian forest growth (Fig. 11b). Additionally, one groundwater table measurement system was installed near the desert station in 2018. The depth of the groundwater table level was approximately 10-11 m in the desert and showed no significant variation over the years (Fig. 11d).

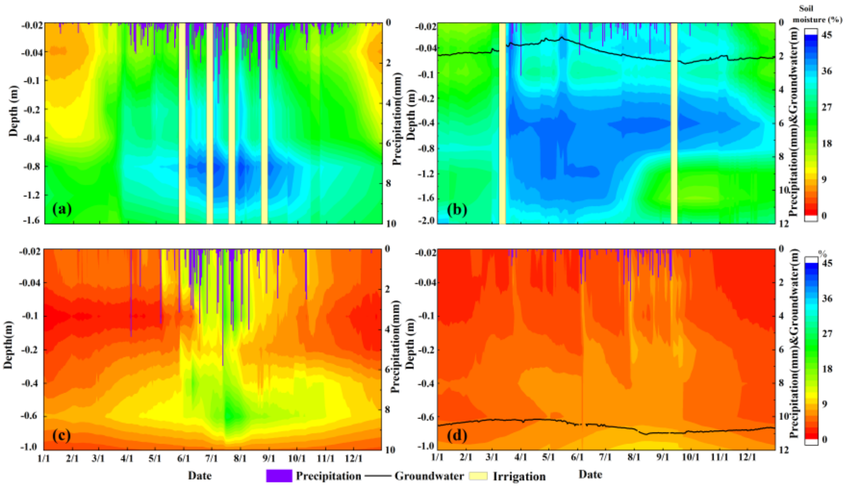

Fig. 11. Comparison of precipitation and soil moisture profile between desert and oasis (2012-2021, a: oasis in the middle reaches (maize, Daman); b: oasis in the lower reaches (*Tamarix*, Sidaoqiao); c: desert in middle reaches (Bajitan Gobi); d: desert in lower reaches (desert))

4.3 Vegetation and soil parameters

The vegetation parameters include photosynthetically active radiation (PAR), leaf area index (LAI), phenology, sun-induced chlorophyll fluorescence (SIF), etc. The PAR, the amount of light available for photosynthesis, is observed at stations with vegetation cover, and it can be used as the source of energy for photosynthesis by green plants.

The PAR observations showed similar seasonal variations in typical oasis ecosystems in the middle and lower reaches, with a maximum daily PAR of approximately 750 μmol m^{-2} s^{-1} (Fig. 14a). Vegetation parameters, such as LAI and phenology, were also observed in the middle and lower reaches. LAI in the middle reaches (maize) increased gradually with crop growth, and it was larger than that in the lower reaches (*Tamarix*), which showed little change in this shrub surface (Fig. 14b). The phenological camera was installed at each station except the desert to acquire the phenology. The greenness index of the green chromatic coordinate (GCC) was derived to capture the key phenological phase of the plant, such as the SOS (start of season), POP (position of peak value), and EOS (end of season) (Fig. 14c).

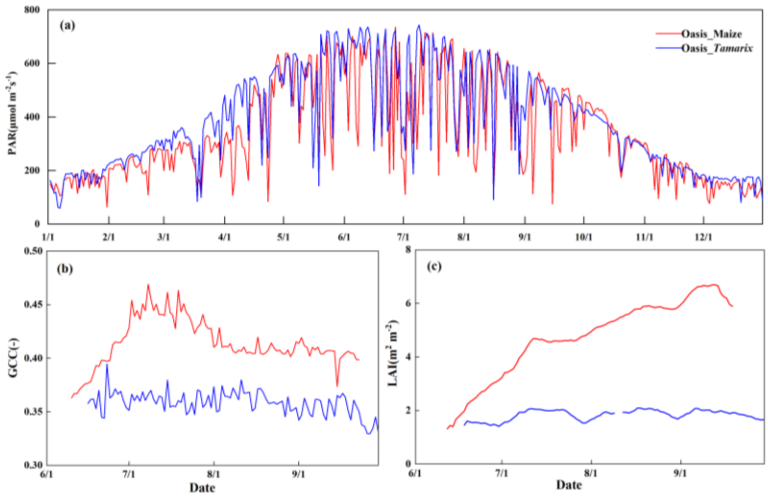

Fig. 12. Variations in vegetation parameters in the middle and lower reaches of the oasis (a, b, c are PAR, LAI and GCC in the artificial and natural oases, respectively, in 2018)

Soil samples were collected at each station in the middle and lower reaches in 2012 and 2020. These soil samples were analyzed in the laboratory, and parameters such as soil texture, porosity, bulk density, saturated hydraulic conductivity, and soil organic matter content were obtained. Some soil parameters at typical stations are shown in Table 3. Silty soil is dominant in the oasis, and sand is dominant in the desert. The porosity and bulk density showed no significant difference. The saturated hydraulic conductivity and soil organic matter at the typical stations are also given in Table 3.

Table 3 Soil parameter measurements at typical stations in 2020

	Station	Soil texture	Soil properties
Middle reaches	Daman (Oasis)	Clay: 6% Silt: 69% Sand: 25%	Porosity: 47.1 %; Bulk density: 1.46 g/cm^3; Saturated hydraulic conductivity: 0.177 mm/min; Saturated water capacity: 64.10 %; PH: 8.48; NH_4^+-N: 0.83 mg/kg; NO_3^--N: 15.90 mg/kg; Soil carbon content: 1.85 %; Soil organic carbon content: 0.72 %; Soil nitrogen content: 0.027%
	Huaizhaizi (Desert)	Clay: 1% Silt: 19% Sand: 80%	Porosity: 38.0 %; Bulk density: 1.49 g/cm^3; Saturated hydraulic conductivity: 4.93 mm/min; Saturated water capacity: 22.21 %; PH: 8.27; $NH4^+$-N: 0.77 mg/kg; NO_3^--N: 29.70 mg/kg; Soil carbon content: 1.83 %; Soil organic carbon content: 0.33 %; Soil nitrogen content: 0.026%
Lower reaches	Sidaoqiao (Oasis)	Clay: 21% Silt: 69% Sand: 10%	Porosity: 45.8 %; Bulk density: 1.47 g/cm^3; PH: 8.80; NH_4^+-N: 1.02 mg/kg; NO_3^--N: 5.23 mg/kg; Soil carbon content: 2.02 %; Soil organic carbon content: 0.70 %; Soil nitrogen content: 0.070%
	Desert around terminal lake (Desert)	Clay: 9% Silt: 7% Sand: 84%	Porosity: 44.4 %; Bulk density: 1.49 g/cm^3; PH: 8.62; NH_4^+-N: 0.26 mg/kg; NO_3^--N: 5.74 mg/kg; Soil carbon content: 1.42 %; Soil organic carbon content: 0.38 %; Soil nitrogen content: 0.039%

5. Data availability

The dataset of energy, water vapor and carbon exchange observations in oasis-desert areas reported in this study, including energy, water vapor and carbon fluxes, hydrometeorological data, and vegetation and soil parameters, are available and can be downloaded freely at the National Tibetan Plateau Data Center (https://doi.org/10.11888/Terre.tpdc.300441, Liu et al., 2023). A specific directory for each observation station was designated with data classified into three categories, namely, energy, water vapor and carbon fluxes, hydrometeorological data, and vegetation and soil parameter data. Short descriptions were also provided for each dataset. The Beijing standard time was used in all the data files (UTC+8).

6. Conclusions

The typical land covers in the middle and lower reaches over the HRB are oases and deserts characterized by fragile environments. Oasiszation and desertification are two opposing processes in arid and semiarid regions with scarce water resources. To combat desertification around oases and maintain the sustainable development of oases, a land surface process integrated observatory network was established in the oasis-desert area in the middle and lower reaches of the HRB. Eleven stations (7 in oasis, 4 in desert) have been established in these regions since 2012 to monitor the energy, water vapor and carbon exchange between land and atmosphere over oasis and desert areas, and a long-term and high-quality oasis and desert dataset of energy, water vapor and carbon fluxes and auxiliary parameters was produced. This study shows the achievements of 11 stations over 10 continuous years of observations, including energy, water vapor and carbon fluxes, hydrometeorology, vegetation and soil parameter data. These data can be used in the analysis of the water-heat-carbon process and its influence mechanism (Wang et al., 2019; Xu et al., 2020; Bai et al., 2021; Wu et al., 2023), calibration and validation of remote sensing products (Ma et al., 2018; Song et al., 2018; Li et al., 2021; Zhang et al., 2022), and simulations of energy, water vapor and carbon exchange (Li et al., 2017b; Liu et al., 2020; He et al., 2022; Zhou et al., 2022). We confirm that the 10-year long-term dataset presented in this study is of high quality with few missing data and believe that the datasets will support ecological security and sustainable development in oasis-desert areas. Most of the stations are ongoing observations, which can play a greater role in such ecologically fragile areas and provide a reference for other similar oasis-desert areas along the Silk Road.

Acknowledgement

This work was supported by the Strategic Priority Research Program of the Chinese Academy of Sciences (Grant no. XDA20100101), the National Natural Science Foundation of China (42171461).

References:

Bai, Y., Liu, Y. L., Kueppers, L. M., Feng, X., Yu, K. L., Yang, X. F., Li, X. Y., and Huang, J. P.: The coupled effect of soil and atmospheric constraints on stress-responses of desert riparian species, Agr. Forest Meteorol., 311, 108701, https://doi.org/10.1016/j.agrformet.2021.108701, 2021.

Che, T., Dai, L.Y., Wang, J., Zhao, K., and Liu, Q: Estimation of snow depth and snow water equivalent distribution using airborne microwave radiometry in the Binggou Watershed, the upper reaches of the Heihe River basin, Int. J. Appl. Earth Obs., 17, 23-32, https://doi.org/10.1016/j.jag.2011.10.014, 2012.

Che, T., Li, X., Liu, S.M., Li, H.Y., Xu, Z.W., Tan, J.L., Zhang, Y., Ren, Z.G., Xiao, L., Deng, J., Jin, R., Ma, M.G., Wang, J., and Yang, X.F.: Integrated hydrometeorological, snow and frozen-ground observations in the alpine region of the Heihe River Basin, China, Earth Syst. Sci. Data, 11, 1483–1499, 2019.

Cheng, G. D., Xiao, D. N., and Wang, G. X.: On the characteristics and building of landscape ecology in arid area, Adv. Geosci., 14 (1), 11–15, 1999. (in Chinese with English abstract).

Cheng, G. D., Li, X., Zhao, W., Xu, Z., Feng, Q., Xiao, S. and Xiao, H.: Integrated study of the water-ecosystem-economy in the Heihe River Basin, Natl. Sci. Rev., 1(3), 413-428, https://doi.org/10.1093/nsr/nwu017, 2014.

Chu, P. C., Lu, S., and Chen, Y.: A numerical modeling study on desert oasis self-supporting mechanisms, J. Hydrol., 312, 256-276, https://doi.org/10.1016/j.jhydrol.2005.02.043, 2005.

Crétaux, J. F., Calmant, S., Romanovski, V., Shabunin, A., Lyard, F., Bergé-Nguyen, M., Cazenave, A., Hernandez, F., and Perosanz, F.: An absolute calibration site for radar altimeters in the continental domain: Lake issykkul in the central asia, J. Geodesy, 83(8), 723-735, http://doi.org/10.1007/s00190-008-0289-7, 2009.

Dregne, H. E.: Global status of desertification, Annals of Arid Zone, 30, 179–185, https://epubs.icar.org.in/index.php/AAZ/article/view/64733, 1991.

Georgescu, M., Moustaoui, M., Mahalov, A., and Dudhia, J.: An alternative explanation of the semiarid urban area “oasis effect”, J. Geophys. Res.-Atmos., 116, D24113, https://doi.org/10.1029/2011JD016720, 2011.

He, X. L., Liu, S. M., Xu, T. R., Yu, K. L., Gentine, P., Zhang, Z., Xu, Z. W., Jiao, D. D., and Wu, D. X.: Improving predictions of evapotranspiration by integrating multi-source observations and land surface model, Agr. Water Manage., 272, 107827, https://doi.org/10.1016/j.agwat.2022.107827, 2022.

Hommeltenberg, J., Mauder, M., Drosler, M., Heidbach, K., Werle, P., and Schmid, H.

P.: Ecosystem scale methane fluxes in a natural temperature bog-pine forest in southern Germany, Agric. For. Meteorol., 198–199, 273–284, https://doi.org/10.1016/j.agrformet.2014.08.017, 2014.

Huang, J. P., Yu, H. P., Guan, X. D., Wang, G. Y., and Guo, R. X: Accelerated dryland expansion under climate change, Nature Clim. Change, 6, 166-171, https://doi.org/10.1038/nclimate2837, 2016.

Liebethal, C., Huwe, B., and Foken, T.: Sensitivity analysis for two ground heat flux calculation approaches, Agric. For. Meteorol., 132(3–4), 253–262, https://doi.org/10.1016/j.agrformet.2005.08.00, 2005.

Li, M. S., Zhou, J., Peng, Z. X., Liu, S. M., Göttsche, F. M., Zhang, X. D., and Song, L. S.: Component radiative temperatures over sparsely vegetated surfaces and their potential for upscaling land surface temperature, Agric. For. Meteorol., 276-277, 107600, https://doi.org/10.1016/j.agrformet.2019.05.031, 2019.

Li, X., Li, X. W., Li, Z. Y., Ma, M. G., Wang, J., Xiao, Q., Liu, Q., Che, T., Chen, E. X., Yan, G. J., Hu, Z. Y., Zhang, L. X., Chu, R. Z., Su, P. X., Liu, Q. H., Liu, S. M., Wang, J. D., Niu, Z., Chen, Y., Jin, R., Wang, W. Z., Ran, Y. H., and Xin, X.: Watershed Allied Telemetry Experimental Research, J. Geophys. Res.-Atmos., 114, D22103, https://doi.org/10.1029/2008JD011590, 2009.

Li, X., Cheng, G. D., Liu, S. M., Xiao, Q., Ma, M. G., Jin, R., Che, T., Liu, Q. H., Wang, W. Z., Qi, Y., Wen, J. G., Li, H. Y., Zhu, G. F., Guo, J. W., Ran, Y. H., Wang, S. G., Zhu, Z. L., Zhou, J., Hu, X. L., and Xu, Z. W.: Heihe Watershed Allied Telemetry Experimental Research (HiWATER): Scientific Objectives and Experimental

Design, B. Am. Meteorol. Soc., 94, 1145–1160, https://doi.org/10.1175/BAMS-D-12-00154.1, 2013.

Li, X., Yang, K., and Zhou, Y.: Progress in the study of oasis-desert interactions, Agric. For. Meteorol., 230, 1-7, https://doi.org/10.1016/j.agrformet.2016.08.022, 2016.

Li, X., Liu, S. M., Xiao, Q., Ma, M. G., Jin, R., Che, T., Wang, W. Z., Hu, X. L., Xu, Z. W., Wen, J. G., and Wang, L. X.: A multiscale dataset for understanding complex eco-hydrological processes in a heterogeneous oasis system, Sci. Data, 4, 170083, https://doi.org/10.1038/sdata.2017.83, 2017a.

Li, X., Zheng, Y., Sun, Z., Tian, Y., Zheng, C. M., Liu, J., Liu, S. M., and Xu, Z. W.: An integrated ecohydrological modeling approach to exploring the dynamic interaction between groundwater and phreatophytes, Ecol. Model., 356, 127-140, https://doi.org/10.1016/j.ecolmodel.2017.04.017, 2017b.

Li, X., Liu, S. M., Li, H. X., Ma, Y. F., Wang, J. H., Zhang, Y., Xu, Z. W., Xu, T. R., Song, L. S., Yang, X. F., Lu, Z., Wang, Z. Y., and Guo, Z. X.: Intercomparison of six upscaling evapotranspiration methods: from site to the satellite pixel, J. Geophys. Res.-Atmos., 123, 6777-6803, https://doi.org/10.1029/2018JD028422, 2018.

Li, X., Liu, S. M., Yang, X. F., Ma, Y. F., He, X. L., Xu, Z. W., Xu, T. R., Song, L. S., Zhang, Y., Hu, X., Qu, Q., and Zhang, X. D.: Upscaling evapotranspiration from a single-site to satellite pixel scale, Remote Sen., 13, 4072, https://doi.org/10.3390/rs13204072, 2021.

Liu, R., Sogachev, A., Yang, X. F., Liu, S. M., Xu, T. R., and Zhang, J. J.: Investigating microclimate effects in an oasis-desert interaction zone, Agric. For. Meteorol., 290, 107992, https://doi.org/10.1016/j.agrformet.2020.107992, 2020.

Liu, S. M., Xu, Z. W., Wang, W. Z., Bai, J., Jia, Z. Z., Zhu, M. J., and Wang, J. M.: A comparison of eddy-covariance and large aperture scintillometer measurements with respect to the energy balance closure problem. Hydrol. Earth Syst. Sci., 15(4), 1291-1306, https://doi.org/10.5194/hess-15-1291-2011, 2011.

Liu, S. M., Xu, Z. W., Song, L. S., Zhao, Q. Y., Ge, Y., Xu, T. R., Ma, Y. F., Zhu, Z. L., Jia, Z. Z., and Zhang, F.: Upscaling evapotranspiration measurements from multi-site to the satellite pixel scale over heterogeneous land surfaces, Agric. For. Meteorol., 230-231, 97-113, https://doi.org/10.1016/j.agrformet.2016.04.008, 2016.

Liu, S. M., Li, X., Xu, Z. W., Che, T., Xiao, Q., Ma, M. G., Liu, Q. H., Jin, R., Guo, J. W., Wang, L. X., Wang, W. Z., Qi, Y., Li, H. Y., Xu, T. R., Ran, Y. H., Hu, X. L., Shi, S. J., Zhu, Z. L., Tan, J. L., Zhang, Y., and Ren, Z.G.: The Heihe Integrated Observatory Network: A basin-scale land surface processes observatory in China, Vadose Zone J., 17, 180072, https://doi.org/10.2136/vzj2018.04.0072, 2018.

Liu, S., Xu, Z., Che, T., Li, X., Xu, T., Ren, Z., Zhang, Y., Tan, J., Song, L., Zhou, J., Zhu, Z., Yang, X., Liu, R., and Ma, Y.: Energy, water vapor and carbon exchange observations in oasis-desert areas of Heihe river basin (2012-2021), National Tibetan Plateau/Third Pole Environment Data Center, https://doi.org/10.11888/Terre.tpdc.300441, 2023.

Ma, Y. F., Liu, S. M., Song, L. S., Xu, Z. W., Liu, Y. L., Xu, T. R., and Zhu, Z. L.:

Estimation of daily evapotranspiration and irrigation water efficiency at a Landsat-like scale for an arid irrigation area using multi-source remote sensing data, Remote sens. environ., 216, 715-734, https://doi.org/10.1016/j.rse.2018.07.019, 2018.

Mao, D., Wang, Z., Wu, B., Zeng, Y., Luo, L., and Zhang, B: Land degradation and restoration in the arid and semiarid zones of China: Quantified evidence and implications from satellites. Land degrad, Dev., 29(11), 3841-3851, https://doi.org/10.1002/ldr.3135, 2018.

Meng, X., Lv, S., Zhang, T., Guo, J., Gao, Y., Bao, Y., Wen, L., Luo, S., and Liu, Y.: Numerical simulations of the atmospheric and land conditions over the jinta oasis in northwestern China with satellite-derived land surface parameters, J. Geophys. Res.-Atmos., 114, 605-617, https://doi.org/10.1029/2008JD010360, 2009.

Potchter, O., Goldman, D., Kadish, D., and Iluz, D.: The oasis effect in an extremely hot and arid climate: The case of southern Israel, J. Arid Environ., 72, 1721-1733, https://doi.org/10.1016/j.jaridenv.2008.03.004, 2008.

Qu, Y. H., Zhu, Y. Q., Han, W. C., Wang, J. D., and Ma, M. G: Crop leaf area index observations with a wireless sensor network and its potential for validating remote sensing products, IEEE J-STARS., 7(2), 431-444, https://doi.org/10.1109/JSTARS.2013.2289931, 2014.

Scanlon, B. R., Keese, K. E., Flint, A. L., Flint, L. E., Gaye, C. B., Edmunds, W. M., and Simmers, I.: Global synthesis of groundwater recharge in semiarid and arid regions, Hydrol. Process, 20 (15), 3335–3370, https://doi.org/10.1002/hyp.6335, 2006.

Stone, K. B.: Burke-Litwin organizational assessment survey: reliability and validity, Organization development journal, 33(2), 33-50, 2015.

Stanev, E., Staneva, J., Bullister, J., and Murray, J.: Ventilation of the black sea pycnocline. Parameterization of convection, numerical simulations and validations against observed chlorofluorocarbon data, Deep sea research part I: Oceanographic research papers, 51 (12), 2137-2169, https://doi.org/10.1016/j.dsr.2004.07.018, 2004.

Stoy, P.C., Mauder, M., Foken, T., Marcolla, B., Boegh, E., Ibrom, A., Arain, M., Arneth, A., Aurela, M., Bernhofer, C., Cescatti, A., Dellwik, E., Duce, P., Gianelle, D., Gorsel, E., Kiely, G., Knohl, A., Margolis, H., McCaughey, H., Merbold, L., Montagnanti, L., Papale, D., Reichstein, M., Saunders, M., Serrano-Ortiz, P., Sottocornola, M., Spano, D., Vaccari, F., and Varlagin, A: A data-driven analysis of energy balance closure across FLUXNET research sites: The role of landscape scale heterogeneity, Agric. For. Meteorol., 171-172, 137-152, http://dx.doi.org/10.1016/j.agrformet.2012.11.004, 2013.

Song, L.S., Liu, S.M., Kustas, W.P., Nieto, H., Sun, L., Xu, Z.W., Skaggs, T.H., Yang, Y., Ma, M.G., Xu, T.R., Tang, X.G., and Li, Q.P.: Monitoring and validating spatially and temporally continuous daily evaporation and transpiration at river basin scale, Remote sens. environ., 219, 72-88, https://doi.org/10.1016/j.rse.2018.10.002, 2018.

Taha, H., Akbari, H., and Rosenfeld, A.: Heat island and oasis effects of vegetative canopies, Theor. Appl. Climatol., 44, 123-138, https://doi.org/10.1007/BF00867999, 1991.

Tagesson, T., Fensholt, R., Cappelaere, B., Mougin, E., Horion, S., Kergoat, L., Nieto, H., Mbow, C., Ehammer, A., Demarty, J., and Ardö, J.: Spatiotemporal variability in carbon exchange fluxes across the Sahel, Agric. For. Meteorol., 226-227, 108-118, https://doi.org/10.1016/j.agrformet.2016.05.013, 2016.

Twine, T.E., Kustas, W.P., Norman, J.M., Cook, D.R., Houser, P.R., Meyers, T.P., Prueger, J.H., Starks, P.J., and Wesely, M.L.: Correcting eddy-covariance flux underestimates over a grassland. Agric. For. Meteorol., 103(3), 279-300, https://doi.org/10.1016/S0168-1923(00)00123-4, 2000.

Wang, J. M., and Mitsuta, Y.: Evaporation from the desert: some preliminary results of HEIFE, Boundary Layer Meteorology, 59, 413-418, https://doi.org/10.1007/BF0221546, 1992.

Wang, G. X., and Cheng, G. D.: Water resource development and its influence on the environment in arid areas of China-the case of the Hei River basin, J. Arid Environ., 43, 121–131, https://doi.org/10.1006/jare.1999.0563, 1999.

Wang, H. B., Li, X., Xiao, J. F., Ma, M. G., Tan, J. L., Wang, X. F., and Geng, L. Y.: Carbon fluxes across alpine, oasis, and desert ecosystems in northwestern China: The importance of water availability, Sci. total environ., 697, 133978, https://doi.org/10.1016/j.scitotenv.2019.133978, 2019.

Wen, X., Lv, S., and Jin, J.: Integrating remote sensing data with WRF for improved simulations of oasis effects on local weather processes over an arid region in northwestern China, J. Hydrometeorol., 13(2), 573-587, https://doi.org/10.1175/JHM-D-10-05001.1, 2012.

Wu, D. X., Liu, S. M., Wu, X. C., Xu, T. R., Xu, Z. W., He, X. L., and Shi, H. Y.:

Evaluation of the intrinsic temperature sensitivity of ecosystem respiration in typical ecosystems of an endorheic river basin, Agric. For. Meteorol., 333, 109393, https://doi.org/10.1016/j.agrformet.2023.109393, 2023.

Xu, Z. W., Liu, S. M., Li, X., Shi, S. J., Wang, J. M., Zhu, Z. L., Xu, T. R., Wang, W. Z., and Ma, M. G.: Intercomparison of surface energy flux measurement systems used during the HiWATER-MUSOEXE, J. Geophys. Res.-Atmos., 118, 13140-13157, https://doi.org/10.1002/2013JD020260, 2013.

Xu, Z.W., Ma, Y.F., Liu, S.M., Shi, W.J., and Wang, J.M.: Assessment of the energy balance closure under advective conditions and its impact using remote sensing data, J. Appl. Meteorol. Clim., 56 (1), 127-140, https://doi.org/10.1175/JAMC-D-16-0096.1, 2017.

Xu, Z. W., Liu, S. M., Zhu, Z. L., Zhou, J., Shi, W. J., Xu, T. R., Yang, X. F., Zhang, Y., and He, X.L.: Exploring evapotranspiration changes in a typical endorheic basin through the integrated observatory network, Agric. For. Meteorol., 290, 108010, https://doi.org/10.1016/j.agrformet.2020.108010, 2020.

Xue, J., Gui, D., Lei, J., Sun, H., Zeng, F., Mao, D., Zhang, Z., Jin, Q., and Liu, Y.: Oasis microclimate effects under different weather events in arid or hyper arid regions: A case analysis in southern Taklimakan desert and implication for maintaining oasis sustainability, Theor. Appl. Climatol., 137, 89-101, https://doi.org/10.1007/s00704-018-2567-5, 2019.

Zhang, Y. Y., and Zhao, W. Z.: Vegetation and soil property response of short-timefencing in temperate desert of the Hexi Corridor northwestern China, Catena, 133, 43–51, https://doi.org/10.1016/j.catena.2015.04.019, 2015.

Zhang, X. Y., Arimoto, R., Zhu, G. H., Chen, T., and Zhang, G. Y.: Concentration, size-distribution and deposition of mineral aerosol over Chinese desert regions, Tellus B: Chemical and Physical Meteorology, 50(4), 317-330, https://doi.org/10.3402/tellusb.v50i4.16131, 2016a.

Zhang, Q., Sun, R., Jiang, G.Q., Xu, Z. W., and Liu, S. M.: Carbon and energy flux from a Phragmites australis wetland in Zhangye oasis-desert area, China, Agric. For. Meteorol., 230-231, 45-57, https://doi.org/10.1016/j.agrformet.2016.02.019, 2016b.

Zhang, Y., Zhao, W., He, J., and Fu, L.: Soil susceptibility to macropore flow across a desert-oasis ecotone of the Hexi Corridor, Northwest China, Water Resour. Res., 54, 1281–1294, https://doi.org/10.1002/2017WR021462, 2018.

Zhang, Z., Poulter, B., Knox, S., Stavert, A., McNicol, G., Fluet-Chouinard, E., Feinberg, A., Zhao, Y., Bousquet, P., Canadell, J., Ganesan, A., Hugelius, G., Jackson, R., Patra, P., Saunois, M., Höglund-Isaksson, L., Huang, C., Chatterjee, A., and Li, X.: Anthropogenic emission is the main contributor to the rise of atmospheric methane during 1993–2017, Natl. Sci. Rev., 9(5), nwab200, https://doi.org/10.1093/nsr/nwab200, 2022.

Zhang, Y., Liu, S. M., Song, L. S., Li, X., Jia, Z. Z., Xu, T. R., Xu, Z. W., Ma, Y. F., Zhou, J., Yang, X. F., He, X. L., Yao, Y. J., and Hu, G. C.: Integrated Validation of Coarse Remotely Sensed Evapotranspiration Products over Heterogeneous Land Surfaces, Remote Sens., 14, 3467, https://doi.org/10.3390/rs14143467, 2022.

Zhao, R., Chen, Y., Shi, P., Zhang, L., Pan, J., and Zhao, H.: Land use and land cover change and driving mechanism in the arid inland river basin: a case study of Tarim River, Xinjiang, China, Environ. Earth sci., 68(2), 591-604, https://doi 10.1007/s12665-012-1763-3, 2013.

Zheng, C., Liu, S. M., Song, L. S., Xu, Z. W., Guo, J. X., Ma, Y. F., Ju, Q., and Wang, J. M.: Comparison of sensible and latent heat fluxes from optical-microwave scintillometers and eddy covariance systems with respect to surface energy balance closure, Agric. For. Meteorol., 331, 109345, https://doi.org/10.1016/j.agrformet.2023.109345, 2023.

Zhou, Y., and Li, X.: Energy balance closures in diverse ecosystems of an endorheic river basin, Agric. For. Meteorol., 274, 118-131, https://doi.org/10.1016/j.agrformet.2019.04.019, 2018.

Zhou, Y., Liao, W., and Li, X.: The contributions of individual factors to the oasis cold island effect intensity in the Heihe River Basin, Agric. For. Meteorol., 312, 108706, https://doi.org/10.1016/j.agrformet.2021.108706, 2022.